BNL-NUREG-32194
CONF-830301--5

BNL-NUREG--32194

DE83 003940

FLOW-EXCURSION-INDUCED ORYOUT AT LOW-HEAT-FLUX NATURAL-CONVECTION BOILING

Mohsen Khatib-Rahbar and Erik G. Cazzoli
Department of Nuclear Energy
Brookhaven National Laboratory
Upton, New York 11973

ABSTRACT

Flow-excursion-induced dryout at low-heat-flux natural-convection boiling, typical of liquid-metal fast-breeder reactors, is addressed. Steady-state calculations indicate that low-quality boiling is possible up to the point of Ledinegg instability leading to flow excursion and subsequent dryout in agreement with experimental data. A flow-regime-dependent dryout heat-flux relationship based upon saturated boiling criterion is also presented. Transient analysis indicates that premature flow excursion can not be ruled out and sodium boiling is highly transient dependent. Analysis of a high-heat-flux forced convection, loss-of-flow transient shows a significantly faster flow excursion leading to dryout in excellent agreement with parallel calculations using the two-dimensional THORAX code.

NOMENCLATURE

A	Flow Cross Sectional Area, m^2
C	Constant in the Friction Factor Correlation
D	Rod Diameter, m
D_e	Equivalent Hydraulic Diameter, m
f	Friction Factor
g	Gravitational Acceleration, m/s^2
h	Fluid Enthalpy, J/kg
h_f	Enthalpy of Saturated Liquid, J/kg
h_g	Enthalpy of Saturated Vapor, J/kg
h_{fg}	Enthalpy of Vaporization ($h_g - h_f$), J/kg
I	Fluid Inertia, m^{-1}
i	Inlet
j	Node Number
K_{in}	Inlet Loss Coefficient
K_o	Outlet Loss Coefficient
L_h	Heated Length
M	Total Number of Nodes
N	Number of Rods Per Assembly
n	Exponent in Friction Factor Correlation
o	Outlet
P	Pressure, N/m2
p_h	Heated Perimeter ($N\pi D$), m
q''	Heat Flux, W/m^2
T	Temperature, K
t	Time, s
W	Mass Flow Rate, kg/s
X_{tt}	Lockhart-Martinelli Parameter
X	Axial Position, m
Z	Elevation, m

GREEK SYMBOLS

α	Void Fraction
Δh_{sc}	Inlet Subcooling ($h_f - h$), J/kg
ΔT_{sc}	Inlet Subcooling ($T_f - T$), k
$\langle\rho\rangle$	Average Density, kg/m^3
ρ_f	Density of Saturated Liquid, kg/m^3
ρ_g	Density of Saturated Vapor, kg/m^3
v_f	Specific Volume of Saturated Liquid, m^3/kg
v_g	Specific Volume of Saturated Vapor, m^3/kg
v_{fg}	($v_f - v_g$), m^3/kg
μ_f	Dynamic Viscosity of Saturated Liquid, $N\text{-}s/m^2$
μ_g	Dynamic Viscosity of Saturated Vapor, $N\text{-}s/m^2$
μ_{fg}	($\mu_f - \mu_g$), $N\text{-}s/m^2$
x	Quality

INTRODUCTION

The Liquid Metal Cooled Fast Breeder Reactors (LMFBR's) are currently designed so that the maximum coolant temperature during normal operation is about 350°K below the saturation temperature. Nevertheless, despite this large temperature margin, hypothetical accidents must be envisioned that would lead to coolant temperature excursions and boiling.

Among the most serious of the postulated accidents are the primary loss-of-piping integrity accident and the complete loss-of-heat sink accident. Analysis models used to calculate the consequences of such accidents assume that once sodium boiling is initiated film dryout occurs as a result of rapid vapor bubble growth and subsequent subassembly flow stagnation or reversal.

There are many factors, such as transient flow redistribution between subassemblies, that will deter-

mine whether flow stagnation and boiling will occur in a particular subassembly in a particular accident (1). Once boiling is initiated in an assembly, a substantial gravity pressure difference would exist between this assembly and other cooler assemblies in the core, giving rise to natural convection flow boiling accompanied by flow oscillations prior to excursion often leading to fuel pin dryout.

Of particular interest to LMFBR safety analysis, is the prediction of sodium boiling behavior and conditions conducive to the fuel pin dryout phenomenon.

Analytical models to date are based on the slug flow approximations developed mainly to describe sodium boiling behavior under conditions of high heat flux forced convection. Application of these types of models to recent experiments (2,3) has shown to be very sensitive to a number of input parameters, such as, liquid film thickness at the time of voiding inception; degree of superheat and wall friction factor (4).

Detailed multidimensional boiling models have also been developed and used to study sodium boiling phenomenon in LMFBR rod bundles (5,6); however, due to the mathematical and numerical complexity of these methods, their application to long duration natural convection transients is not very practical.

It is therefore, the principal objective of the present work to formulate an analysis method of for study of low heat flux sodium boiling, in particular prediction of fuel pin coolability and dryout limits during natural convection transient events in LMFBRs(7).

SODIUM BOILING AND FLOW EXCURSION PHENOMENON

The low pressure operation of sodium cooled fast reactors compared with light water reactors influences the overall pressure drop characteristic during boiling. With a high pressure system it is possible to have a single valued pressure drop-flow characteristic for a boiling channel, but with low pressure systems this is not so.

Figure 1 illustrates the difference between low and high pressure boiling systems. It is seen for the low pressure system that the flow rate can be multivalued for certain available pressure characteristics. The increase of the pressure drop as the flow is reduced to cause boiling is due to an increase in the frictional component and the requirement of extra pressure head to produce the necessary acceleration from the single-phase fluid to a two-phase mixture. Both these terms decrease as the system pressure increases, and consequently at a sufficiently higher pressure there is no increase in the pressure drop as the flow is reduced to produce boiling (8).

For low pressure sodium boiling, the implications of the S-curve shown in Fig. 1a are that at the onset of boiling a flow excursion could take place and possibly cause the Critical Heat Flux (CHF) conditions to be exceeded.

The flow excursion instability also referred to as Ledinegg instability (9,10) can be explained using a simple momentum balance equation of the form:

$$I \frac{dW}{dt} = (\Delta P)_{EXT} - (\Delta P)_{int} \qquad (1)$$

where W is the coolant mass flow rate, I is the fluid inertia (L/A), $(\Delta P)_{int}$ is the channel internal pressure drop due to friction, spatial acceleration, buoyancy, inlet and outlet orifices, and $(\Delta P)_{EXT}$ is the driving pressure differential.

For a small perturbation around an equilibrium point W_o,

$$W = W_o + \delta W \qquad (2a)$$

$$(\Delta P)_{int} = \left[(\Delta P)_{int}\right]_{W_o} + \frac{\partial}{\partial W}\left[(\Delta P)_{int}\right]_{W_o} \delta W \qquad (2b)$$

$$(\Delta P)_{EXT} = \left[(\Delta P)_{EXT}\right]_{W_o} + \frac{\partial}{\partial W}\left[(\Delta P)_{EXT}\right]_{W_o} \delta W \qquad (2c)$$

The following solution for the flow perturbation can be obtained:

$$\delta W = \delta W_o \exp(\xi t/I) \qquad (3)$$

where

$$\xi = \left[\frac{\partial}{\partial W}(\Delta P)_{EXT} - \frac{\partial}{\partial W}(\Delta P)_{int}\right]_{W_o} \qquad (4)$$

Equation (3) shows that the perturbation δW_o will grow if ξ is positive. In other words the system will be unstable if the slope of the internal pressure drop is more negative than the slope of the external pressure differential. For natural convection boiling, the slope of the external pressure drop is zero, hence, instabilities can occur for any negative slope of the internal characteristic.

Equation (3) shows that the flow excursion process is a transient phenomenon and its time constant is directly related to the fluid inertia and pressure drop characteristics. At natural convection boiling conditions the value of increases with increasing heat flux; and therefore the flow excursion process will take place over a much shorter duration at higher heat flux levels, as demonstrated later in this paper.

The time-dependent momentum equation was used to derive the stability criterion of equation (4), however, the criterion itself (negative value of ξ) is based on steady-state considerations only.

Figure 2a shows typical pressure-drop versus flow rate and heat flux characteristics for sodium under natural convection conditions. The intersections of these curves with the external pressure differential ΔP_{EXT} (horizontal line) represent possible operating conditions.

Figure 2b illustrates all possible solutions in terms of mass flow rate and heat flux. The dashed line indicates the unstable operating points while the solid lines show the stable conditions. It is therefore evident that for certain values of heat flux, multiple solutions exist for the mass flow rate and thus the operating condition is highly dependent on the past history.

Steady state single-phase and two-phase natural convection behavior of channel flows can be examined through solution of the steady state energy and momentum equations of the form:

$$h_j = h_{j-1} + \frac{N\pi D \Delta X_j q''_j}{W} \qquad j = 2,3,\ldots,M \qquad (5)$$

and

$$\Delta P = \frac{1}{2}\left(\frac{W}{A}\right)^2 \left[\sum_{j=2}^{M} \frac{\phi_j f_j \Delta X_j}{D_e \rho_f} + \left(\frac{(1-x_o)^2}{\rho_f(1-\alpha_o)} + \frac{x_o^2}{\rho_g \alpha_o} - \frac{1}{\rho_i}\right) + \frac{K_{in}}{\rho_i} + \frac{K_o \phi_o}{\rho_f}\right] + g \sum_{j=2}^{M} \langle \rho_j \rangle \Delta Z_j \qquad (6)$$

The two-phase flow multipliers are defined as (11):

$$\phi_j = \left(1 - x_j \frac{v_{fg}}{v_f}\right) \left(1 + x_j \frac{\mu_{fg}}{\mu_g}\right)^{-0.25} \quad (7a)$$

$$\phi_o = 1 + \frac{v_{fg}}{v_f} x_o^{1.5} \quad (7b)$$

The void fraction, α is determined using the following relation (12):

$$\alpha = \frac{1}{1 + 0.28 X_{tt}^{0.71}} \quad (8)$$

where the two-phase flow modulus also known as the Lockhart-Martinelli parameter is defined as:

$$X_{tt} = \left(\frac{1-x}{x}\right)^{0.9} \left(\frac{\rho_g}{\rho_f}\right)^{0.5} \left(\frac{\mu_f}{\mu_g}\right)^{0.1} \quad (9)$$

The Lockhart-Martinelli void fraction relation, approximated by equation (8) has been found to be in excellent agreement with the recent liquid metal test data as discussed by Costa (13).

The single-phase friction factor is defined by:

$$f = C\, Re^{-n} \quad (10)$$

where n = 1 for laminar flow and n = 0.25 for turbulent flow.

For laminar flow through wire-wrapped fuel assemblies C is measured to be constant and equal to 84 (14). On the other hand for turbulent flow C is a complicated function of the pitch to diameter ratio and the spiral wire lead as correlated recently (15,16).

For single-phase (subcooled or superheated) flow, equation (6) is appropriately modified by setting Φ_j, and Φ_o to 1.0 and the density to its single phase value.

The operational regimes identified in Fig. 2 illustrate that single phase natural convection flow exists along the curve ON and the flow rate and enthalpy rise can be derived by solving eqs. (5), (6) and (10) along with an equation of state for density to obtain (17):

$$W \sim q''^{1/(3-n)}, \quad (11)$$

and

$$\Delta h \sim q''^{(2-n)/(3-n)} \quad (12)$$

Equations (11) and (12) indicate the importance of the flow regime change during natural convection cooling, that is for laminar flow both W and Δh are proportional to the $\sqrt{q''}$; while for turbulent flow $W \sim q''^{0.36}$ and $\Delta h \sim q''^{0.64}$. Therefore it is essential to include the Reynolds number dependence for accurate prediction of natural convection behavior (17).

The boiling regimes identified on Fig. 2-2 consist of:

Low Quality Boiling Mode (Line NE) - The operating points on this line correspond to the stable ($\xi < 0$) low quality boiling regime. At E boiling becomes unstable and flow excursion takes place.

Unstable Boiling Mode (R'N"E) - Operation along this curve is statically unstable ($\xi > 0$) and can lead to flow excursion. Also, due to the close proximity of the low quality boiling (Line NE) and the unstable boiling mode solutions, operation with boiling in this heat flux range is expected to be oscillatory in nature, and can often lead to premature excursion.

Stable High Quality Mode (R'N'D E') - Vapor quality along this path is high and the fluid approaches saturated vapor condition at D, at which point enthalpy burnout takes place. Therefore, stable operation beyond D is considered unsafe, and can cause fuel pin failure. Furthermore at R' the flow is unstable and can recover to high flow natural convection leading to restoration of single-phase flow.

Therefore, the heat flux corresponding to the intersection of the saturated vapor line (x_o = 100%) and the high quality curve is of special significance. An approximate analytical solution for this intersection can be found, assuming that the non-boiling length is much smaller than the total length (very small inlet subcooling). Solving the coolant momentum equation for the condition that exit quality is 100% and using an all vapor friction factor one obtains (7):

$$W \simeq \rho_g A \left[\frac{2g\,(\rho_f - \rho_g)\, D_e^{1+n}}{C\, \mu_g^n\, \rho_g^{1-n}}\right]^{(1/2-n)} \quad (13)$$

In other words, in order to maintain a dried-out region in the upper part of the rod bundle, the vapor production rate in the lower part of the rod bundle must be sufficient to maintain voiding and thus prevent reentry of liquid for rewetting, and therefore, the heat flux corresponding to this vapor production rate is termed the "dryout heat flux" and is determined by substituting equation (13) into the energy equation to obtain:

$$q''_{Dryout} \geq \left[\frac{2g\,\rho_g\,(\rho_f - \rho_g)\, D_e^{1+n}}{C\mu^n_g}\right]^{1/(2-n)} \frac{A}{\pi N D L_h} (\Delta h_{sc} + h_{fg}) \quad (14)$$

Again, the influence of flow regime[1] is clearly evident. Equations (13) and (14) are similar to the reentry criterion proposed by Dunn (18) and later modified by Fauske and Ishii (19). These equations treat the flow regime explicitly, and as such the vapor production rate and subsequently the heat flux does not depend on the magnitude of the Reynolds number, but only on its range (turbulent, transition or laminar).

The dryout heat flux approximated by Eq. (14) will be compared to the detailed numerical solution of the energy and momentum equations (Eqs. (5) through (10)) to assess its range of validity for low heat flux natural convection boiling.

[1] In this context, throughout this paper, "flow regime" refers to turbulent, laminar and transition flow regimes.

STEADY STATE ANALYSIS

The steady state model described in the previous section is used to study the sodium boiling characteristics of the Clinch River Breeder Reactor Plant (CRBRP)(20) fuel assembly, and the Oak Ridge National Laboratory Sodium Boiling Test (SBT) system (2).

The CRBRP fuel assemblies consist of 217 pins arranged in a triangular configuration. Figure 3 illustrates the steady state pressure drop versus flow rate characteristics at an average power density of 150 MW/m^3 (4.87 kw/pin or 19.5 W/cm^2). Also shown is the importance of various components of the pressure drop. The S-shape behavior, typical of low pressure boiling discussed earlier, is clearly evident.

Figure 4 shows the pressure drop versus flow rate characteristics at various power densities. The intersection of these curves with the constant, convective driving head provide the possible operating conditions shown in Fig. 5.

Single-phase natural convection flow exists for steady power densities up to 160 MW/m^3 (5.2 kw/pin). Low quality stable boiling occurs for power densities greater than 160 MW/m^3 up to the critical power density of 200 MW/m^3 (6.5 kw/pin or 26 W/cm^2) beyond which, flow excursion leading to enthalpy burnout takes place. Recovering from high-quality low-flow condition is not possible until the power density is reduced to about 44 MW/m^3 (1.43 kw/pin).

Figure 5 also illustrates that the two-phase unstable mode solutions are very close to the stable low quality mode solutions; however, boiling is expected to take place as a result of different power and flow decay characteristics during transient operation. Furthermore premature flow excursions at power densities beyond 57 MW/m^3 (1.83 kw/pin or 7.3 W/cm^2) will lead to film dryout and subsequent cladding temperature excursions.

The boiling map exemplified by Fig. 5 demonstrates a very important characteristic, that, sodium boiling phenomenon is strongly path dependent. Let us consider a case where a system is operating at low power, single-phase natural convection; increasing the power level in small quasi-steady steps leads to an increase in the convective flow along the single-phase natural convection curve. However, if the power level is increased in a large step or ramp, the system can easily move to the right of the two-phase unstable operating curve and thus undergo a premature excursion. A similar situation arises during constant power, variable flow conditions, such as flow coastdown at decay power levels or protected loss-of-piping integrity accidents.

Factors influencing the system operating characteristics during boiling include inlet and outlet orifice losses, and the inlet subcooling.

An enlargement in inlet restriction increases single-phase flow friction and thus provides a damping effect which increases the system stability. A restriction at the exit of a boiling channel increases two-phase friction, which in turn reduces the system stability.

The impact of subassembly inlet subcooling is demonstrated in Figures 5 through 7. Higher sodium inlet temperature reduces the margin to boiling inception and this lowers the point of sodium flow excursion. However, the heat flux interval between the flow excursion and the rewetting process is reduced as the inlet temperature is increased. It must be noted that a significant increase in the subassembly inlet temperature can occur during loss-of-heat sink accidents.

A similar analysis is performed for the ORNL single-channel sodium boiling experiments.

The geometric characteristics of the SBT test section are approximately equal to those of a full scale LMFBR fuel assembly (2). It consists of a radiant furnace heated region, followed by the simulated fission gas plenum region downstream of the heated zone.

Figure 8 shows the calculated boiling map corresponding to the SBT operating conditions. Table III summarizes the test results as compared to the present calculations and those predicted by the SAS3D computer code (4).

Experimentally, single-phase free convection behavior was observed for test section power densities less then 125 MW/m^3. Due to a high degree of wall superheat (100K), a precise determination of boiling inception was not possible. To circumvent this operational problem, argon bubbles were injected upstream of the heated section to induce boiling, once boiling was established, the argon injection was terminated.

A chugging instablity was observed for test section power densities between 125 to 162 MW/m^3. This is attributed to the high degrees of superheat and associated lack of nucleation sites (2,9).

A stable boiling behavior was observed for periods up to 45 minutes at power densities between 162 and 200 MW/m^3. The flow was observed to be stable in the dynamic sense but highly oscillatory. Evidence of more than one operating condition for the same test section power density was also observed for power densities near the lower end of the stable boiling regime.

At test section power densities above 200 MW/m^3, intermittent dryout conditions were encountered. Recovery from dryout was frequently observed.

The above experimental observations are in direct agreement with analysis of the steady state model also summarized in Table I and shown in Fig. 8. The disagreements are in part due to the inaccuracies in the test section power measurement which are shown (2) to be about 45% at 40 MW/m^3 and drop to around 18% at 200 MW/m^3.

It is important to note that the SBT experiment was performed in a quasi-steady state fashion, where the test section power was increased slowly leading to natural convection boiling. Even though it is highly non-prototypic in many ways, it still demonstrates many important characteristics of low pressure boiling typical of LMFBR systems.

DRYOUT CRITERION

It is evident from the computational results supported by experimental data, that enthalpy burnout is expected to take place following flow excursion for heat flux levels greater than q''_{dryout}.

Following flow excursion, the flow rate reduces to a level corresponding to the laminar-turbulent transition regime where $C \sim 0.4$ and $n = 0.25$ (16); thus equation (14) becomes:

$$q''_{dryout} \geq \left[\frac{5g\,\rho_g\,(\rho_f - \rho_g)\,D_e^{1.25}}{\mu_g^{0.25}} \right]^{0.57} \frac{A}{\pi N D L_h} (\Delta h_{sc} + h_{fg}) \qquad (15)$$

Table II summarizes the calculated heat flux limits for the CRBRP fuel assembly discussed in the previous section. Also given is the approximate dryout heat flux limit determined from equation (15) at various inlet subcooling conditions.

It is seen that the dryout heat flux approaches the heat flux corresponding to the point of flow excursion, in the absensce of inlet subcooling. Furthermore, comparison of the detailed numerical solution with those obtained from equation (15) for dryout heat flux show that, the heat flux calculated from the approximate equation is conservative.

These results indicate that the decay heat may be removed via coolant boiling for decay power levels in the range of 3.7% (of nominal) at zero inlet subcooling and up to about 5% (of nominal) at maximum inlet subcooling of 527°K, somewhat higher than those obtained by Dunn (18) and Perkins and Bari (21) for the FFTF reactor using the SAS3D computer code.

Recent calculations reported by Fauske and Ishii (19), using a similar approximate equation and an empirical correlation based on the Katto's low flow convection CHF equation, predict dryout at heat flux levels which are higher than those given in Table II. This discrepancy is believed to be, in part, due to the smaller vapor phase friction factor assumed in the Fauske/Ishii analysis, and to a lesser extent to the difference in the thermodynamic properties.

TRANSIENT ANALYSIS

The analysis presented in the previous section was based on steady state or quasi-steady low heat flux natural convection conditions in LMFBRs. It was shown for the case of CRBRP, that Ledinegg instability will occur at a heat flux greater than 26 W/cm^2; however, any premature excursions will lead to film dryout for heat fluxes greater than 7 W/cm^2. It is therefore essential that the flow excursion takes place prior to the occurrence of dryout.

In order to examine the transient dependence of the Ledinegg instability and subsequent low flow operation, a transient model is developed and used to study this phenomenon.

The model is based on solution of the conservation of mass, momentum and energy equations of the form:

$$\frac{\partial \rho}{\partial t} + \frac{1}{A}\frac{\partial W}{\partial X} = 0 \qquad (16)$$

$$\frac{1}{A}\frac{\partial W}{\partial t} + \frac{1}{A^2}\frac{\partial}{\partial X}\left(\frac{W^2}{\rho^*}\right) + \frac{f}{2\rho D_e A^2} W|W| + \rho g + \frac{\partial P}{\partial X} = 0 \qquad (17)$$

and

$$\rho \frac{\partial h}{\partial t} + \frac{W}{A}\frac{\partial h}{\partial X} = \frac{P_h}{A} q'' \qquad (18)$$

The sonic effects associated with the fluid compressibility can be eliminated by assuming that fluid density may be evaluated as a function of fluid enthalpy only (22,23):

$$\rho = \rho(h, P^*) \qquad (19)$$

where P* is a spatially average reference pressure defined as

$$P^* = 0.5\,(P_{in} + P_{out}) \qquad (20)$$

The assumption of equation (20) is valid, because following pump failure the pressure drop across the reactor drops significantly and thus can be neglected for physical property evaluation.

Furthermore, the thermal expansion effect in the single-phase liquid region is neglected, $\frac{\partial W}{\partial X} = 0$.

These differential equations along with appropriate spatially averaged flow and density relationships are transformed to the equivalent semi-implicit finite difference equations and solved simultaneously with the fuel and structure thermal conduction equations for N - parallel channels, to simulate the transient conditions in LMFBRs (7), using the homogeneous two-phase flow multiplier (Eq. 7) and the Lockhart-Martinelli slip flow correlation (Eq. 8).

Figures 9 and 10 illustrate a typical CRBRP response to a postulated loss-of-forced cooling with reactor scram. It is seen that the coolant flow rate decreases and reaches a minimum and the corresponding coolant temperatures in the reactor increase ("Transition Phase") and eventually start to decrease as the natural circulation flow is established. It is seen that the maximum hot channel temperatures are well below saturation. However, as a result of power to flow ratios much larger than unity in certain transients, such as a loss-of-piping integrity accident, the coolant saturation limit may be exceeded; quasi-steady analysis, typical of those preformed earlier, can not predict such a transient dependent behavior.

To demonstrate these effects as well as the transient dependence of the flow excursion process often leading to premature excursion, loss-of-forced cooling transients in the CRBRP at high power densities (larger than what exists due to decay heating following reactor shutdown) are simulated.

Figures (11) through (13) show the transient results for the decay heat level corresponding to 4.7 kw/pin.

The sodium temperatures increase and reach saturation as a result of power to flow mismatch in the subassembly, leading to low quality boiling at the boundary between the fuel and upper axial blanket regions (Fig. 12).

The boiling region propagates upward causing a significant increase in the fluid buoyancy and thus improvement in the natural convection flow which will eventually sweep the two-phase front out of the assembly, thus restoring the single-phase natural convection flow. Figure 13 shows the sodium inlet and outlet flow rates, illustrating the flow oscillations foreseen by the steady state analysis.

Comparisons to the steady state predictions demonstrate the inadequacy of the steady state calculations in predicting sodium boiling at this power level, however the final quasi-steady natural convection flow and temperature rise was well predicted by the steady state model.

The boiling instability at this heat flux range can be demonstrated if the decay heat level is increased by a very small fraction to about 4.8 kw/ pin.

Figure 14 illustrates that the system undergoes a premature flow excursion causing rapid downward propagation of the voided region and subsequent temperature excursions (Fig. 15) as a result of the reduction in sodium mass flow rate and thus leading to enthalpy burnout also predicted by the steady state analysis.

Figure (14) also demonstrates that, at low heat flux, the flow excursion process is rather slow; and it occurs over a 10 to 20 second time frame, in agreement with the experimental observations reported by Costa (13).

These results testify to the degree of the transient dependence of the flow excursion process. It is seen that premature flow excursion can not be ruled out, particularly, for severe transients where the flow rate may be changing quite rapidly; however, there is a possibility of maintaining low quality oscillatory boiling for an extended period as demonstrated in recent ORNL rod bundle experiments (24).

Therefore, it can be safely assumed that permanent fuel pin dryout can be avoided prior to flow excursion. Furthermore, even if flow excursion does take place, the heat flux must be sufficiently high to cause film dryout ($q'' > q''_{Dryout}$).

The influence of slow heat-up of the primary system sodium, typical of loss-of-heat sink accidents with reactor scram, is being investigated to determine the extent of decay heat removal due to the high quality boiling following flow excursion (provided it occurs) prior to core uncovery.

HIGH HEAT FLUX BOILING

The flow excursion process for high heat flux forced circulation systems is also governed by the Ledinegg instability criterion of Eq. (4), however, due to the small contribution of the thermal buoyancy head, to the total system pressure drop at high heat flux, high flow rate conditions, the unstable boiling mode is even closer to the low quality boiling mode solution. Therefore, premature excursion is much more likely as compared to the low heat flux natural convection boiling.

It has been long recognized that two-dimensional effects dominate sodium boiling process, especially in small bundles having large edge clearance (5,6). However as the bundle size increases thereby reducing the edge fraction, the boiling process becomes increasingly one-dimensional. It has been demonstrated by Dearing (5), and supported by ORNL-THORS experiments, that in going from a 19 pin bundle (45% edge) to a 217 pin bundle (21% edge) the time to flow excursion is reduced by about a factor six.

In order to demonstrate the validity of the present model, and its applicability to typical LMFBR rod bundles at high heat flux, the model is used to simulate a loss-of-flow transient in a 217 pin bundle operating at 15 kw/pin, 2 M/S sodium inlet velocity and 663 K sodium inlet temperature. The results are then compared with those reported by Dearing (5) using the two-dimensional Porous Blockage Code, THORAX.

Loss-of-flow is simulated by changing the driving head according to:

$$\Delta P(t) = \begin{cases} \Delta P(t=0)\ (1 - 0.144t) & 0 \le t \le 3.6\ s \\ 0.48\ \Delta P(t=0) & t > 3.6\ s \end{cases} \qquad (21)$$

Figure (16) shows the axial position of the voiding propagation in the bundle. It is seen that Ledinegg instability begins at the time when a large fraction of the bundle is voided leading to rapid flow excursion as illustrated by Fig.(17). Furthermore, film dryout is predicted to occur at about 5.5 seconds following boiling inception in excellent agreement with the two-dimensional THORAX calculations.

Comparison of the flow excursion process for high and low heat flux boiling, clearly indicates that the severity of flow excursion increases with increasing power level as a result of faster propagation of the boiling region inside the bundle. Furthermore, under low heat flux natural convection boiling conditions (generally much slower than high heat flux boiling), the thermal inertia of the subassembly structural material can play a significant role in the boiling propagation.

SUMMARY AND CONCLUSIONS

Flow-excursion-induced dryout at low heat flux natural convection sodium boiling, typical of liquid metal fast breeder reactor following loss-of-forced cooling with reactor shutdown, was addressed.

Steady state predictions show that low quality sodium boiling is possible up to the point of Ledinegg instability leading to flow excursion and subsequent film dryout in agreement with ORNL-SBT data.

It was also demonstrated that due to the close proximity of the low quality and unstable boiling modes, premature excursions can limit extended operation up to the point of Ledinegg instability and hence lead to enthalpy burnout, provided the heat flux level is higher than that corresponding to the saturated boiling.

A flow regime-dependent approximate heat flux relationship corresponding to the limit of safe operation was presented, and comparisons with exact numerical solutions at various inlet subcooling demonstrated good agreement in the conservative direction.

Transient calculations showed, the strong transient dependence of the flow excursion process, in particular the impact of system distrubances on premature excursion, flow excursion induced dryout for heat flux levels greater than saturated, low flow convection heat flux can not be ruled out.

Furthermore, the transient model was used to simulate a high heat flux-forced circulation loss-of-flow transient, and comparisons were made to parallel calculations using the validated two-dimensional THORAX code.

Premature flow excursion may preclude operation up to the limit of Ledinegg instability if sodium boiling could be avoided in the first minutes after reactor scram, subsequent boiling could remove sufficient decay heat to prevent cladding failure provided core uncovery has not taken place; this is in agreement with studies concluded recently (19). Furthermore, the inclusion of the flow regime dependence on the dryout heat fluxes proposed in this paper significantly influences the accurate prediction of the safe heat flux limits.

ACKNOWLEDGMENT

The authors wish to extend their appreciation to Professor John E. Meyer of the Massachusetts Institute of Technology for numerous technical discussions and his valuable advice throughout this study.

Thanks are due to Dr. Akira Watanabe and Mr. Nobuo Tanaka of the Power Nuclear and Fuel Development Corporation (PNC) of Japan for providing partial financial support of this project and to Mrs. Carmen Falkenbach for typing the manuscript.

The work reported here was also supported in part by the Division of Accident Evaluation, United States Nuclear Regulatory Commission.

REFERENCES

1. M. Khatib-Rahbar, J. G. Guppy, and A. K. Agrawal, "Hypothetical Loss-of-Heat-Sink and In-Vessel Natural Convection: Homogeneous and Heterogeneous Core Designs", in Decay Heat Removal and Natural Convection in Fast Breeder Reactors, A. K. Agrawal and J. G. Guppy (Ed.), Hemisphere Publishing Co. (1981).

2. P. W. Garrison, R. H. Morris, and B. H. Montgomery, "Dryout Measurements for Sodium Natural Convection in a Vertical Channel", Oak Ridge National Laboratory, ORNL/ TM-7018 (1979).

3. R. J. Ribando et. al., "Sodium Boiling in a Full-Length 19-Pin Simulated Fuel Assembly (THORS Bundle 6A)", Oak Ridge National Laboratory, ORNL/TM-6553 (1979).

4. G. Klein and F. Dunn, "SAS3D Analysis of Natural-Convection Boiling Behavior in the Sodium Boiling Test Facility", Trans. Am. Nucl. Soc. 33, (1979), p. 517.

5. J. F. Dearing, "Two-Dimensional Computational Modeling of Sodium Boiling in Simulated LMFBR Fuel Pin Bundles", Trans. Am. Nucl. Soc. 38, (1981), p. 755.

6. A. L. Schor and N. E. Todreas, "A Four Equation Two-Phase Flow Model for Sodium Boiling Simulation of LMFBR Fuel Assemblies", Proceeding of 10th Liquid Metal Boiling Working Group, H.M. Kottowski and W. Peppler (Eds.), Karlsruhe, Federal Republic of Germany (1982)

7. M. Khatib-Rahbar and E. G. Cazzoli, "Modeling and Analysis of Low Heat Flux Natural Convection Sodium Boiling in LMFBRs", BNL-NUREG-51541 (March 1982).

8. R. T. Lahey, Jr., "The Analysis of System Pressure Drop Characteristics During Flow Boiling", Trans. Am. Nucl. Soc. 38, (1981), p. 770.

9. J. A. Bour'e et. al., "Review of Two-Phase Flow Instabilities", Nucl. Eng. and Design 25, (1973), p. 165.

10. G. Yadigaroglu, "Two-Phase Flow Instabilities and Propagation Phenomena", in Thermohydraulics of Two-Phase Systems for Industrial Design and Nuclear Engineering, J. M. Delhaye, M. Giot, and M. L. Riethmuller (Eds.), Hemisphere Publishing Co. (1981).

11. J. G. Collier, Convective Boiling and Condensation, McGraw-Hill Book Co., UK, (1972).

12. D. Butterworth, "A Comparison of Some Void-Fraction Relationships for Co-Current Gas-Liquid Flow", Int. J. of Multiphase Flow, 1, (1975), p. 845.

13. J. Costa, "Contribution to the Study of Sodium Boiling During Slow Pump Coastdown in LMFBR Subassemblies", in Symposium on the Thermal and Hydraulic Aspects of Nuclear Reactor Safety Vol. 2, O. C. Jones, Jr., and S. G. Bankoff (Eds.), ASME, New York (1978).

14. S. L. Additon and E. A. Parziale, "Natural Circulation in FFTF, A Loop-Type LMFBR", in Symposium on the Thermal and Hydraulic Aspects of Nuclear Reactor Safety, Vol. 2, O. C. Jones, Jr. and S. G. Bankoff, (Eds.), ASME, York (1977).

15. E. H. Novendstren, "Turbulent Flow Pressure Drop Model for Fuel Rod Assemblies Utilizing a Helical Wire-Wrap Space System", Nucl. Eng. & Design 22, (1972), p. 19.

16. D. R. Spencer and R. A. Markley, "Friction Factor Correlation for 217-Pin Wire-Wrap-Spaced LMFBR Fuel Assemblies", Trans. Am. Nucl. Soc. 39, (1981), p. 1014.

17. A. K. Agrawal, M. Khatib-Rahbar, and I. K. Madni, "Prediction of Decay Heat Removal Capabilities for LMFBRs and Comparison with Experiments", Nucl. Eng. & Design 66, (1981), p. 437.

18. F. E. Dunn, "Severe FFTF Natural Ciurculation Transients with Boiling", ANL/RAS 76-26 (Sept. 1976).

19. H. K. Fauske and M. Ishii, "Sodium Re-entry and Dryout Criteria Under Decay Power Conditions", Proceedings of the International Meeting on Liquid Metal Fast Breeder Reactor Safety and Related Design and Operational Aspects, Lyon-Ecully, France, July 19-23, 1982.

20. Clinch River Breeder Reactor Plant, Preliminary Safety Analysis Report, Project Management Corporation (1975).

21. K. R. Perkins and R. A. Bari, "SAS-3D Evaluation of Boiling at Decay-Heat Levels in FFTF", Trans. Am. Nucl. Soc. 33, (1979), p. 516.

22. J. E. Meyer, "Hydrodynamic Models for the Treatment of Reactor Thermal Transients", Nucl. Sci. and Eng. 10, (1961), p. 269.

23. M. Ishii and O. C. Jones, Jr., "Derivation and Application of Scaling Criteria for Two-Phase Flows", NATO Advanced Study Institute on Two-Phase Flows and Heat Transfer, Session 1C, Istanbul, Turkey, August 16-27, 1976.

24. S. D. Rose, et al., "Analysis of Natural Convection Sodium Boiling in a 61-Pin Simulated LMFBR Fuel Assembly", Proceedings of 10th Liquid Metal Boiling Working Group, H.M. Kottowski and W. Peppler (Eds.), Karlsruhe, Federal Republic of Germany (1982).

Table I SBT Natural Convection Test Results

Test No.	q (kW/m²)	Experiment (kg/m²-s)	Prediction (kg/m²-s) Low K	Intermediate	High K	Comments Experimental	Present model	Lahey
10702	37	72	102	--	--	Single Phase Natural Convection	Single Phase Natural Convection	Single Phase Natural Convection
10901	42	225	113	--	--			
10902	62	93	134	88	21			
10003	87	103	160	133	18			
10002	87	93	160	133	18			
10004	100	111	171	154.5	17.3			
13101	125	--	207.7	201.5	17.3			
13201	137	--	227.5	222.5	17.3	Chugging		
11001	162	247	268.5	265.5	17.3		Steady Boiling	Steady Boiling
12901	162	103	268.5	265.5	17.3			
12101	174	82	287.5	287.5	17.3	Steady Boiling		
12501	174	93	287.5	287.5	17.3			
12502	174	72	287.5	287.5	17.3			Rewet
12701	186	82	--	--	17.3			
12001	186	247	--	--	17.3		Dryout	
11901	199	113	--	--	17.3			
12002	199	93	--	--	17.3			
12201	199	--	--	--	17.3			
12001	211	93.31	--	--	17.3			
12301	211	72.41	--	--	17.3	Dryout		Dryout
12401	211	--	--	--	17.3			
12601	211	--	--	--	17.3			

Table II Comparison of Heat Flux Limits

T_{in}(k)	ΔT_{sc}(k)	q" (W/cm²) Excursion	q"(W/cm²) Dryout Numerical	q"(W/cm²) Dryout Eq. (15)	Error(%)
673	527	25.7	7.30	6.4	14
873	327	15.3	6.15	6.0	3
1073	127	5.8	5.35	5.4	1

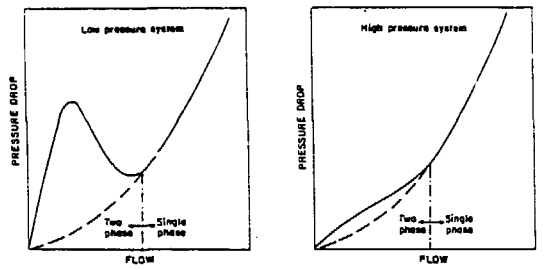

Figure 1 Pressure Drop Characteristics of (a) Low Pressure, and (b) High Pressure Systems During Flow Boiling

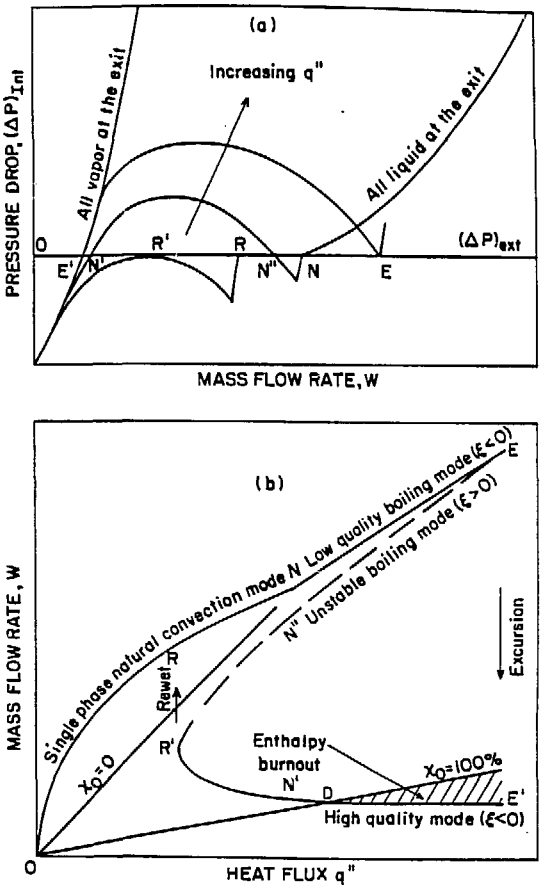

Figure 2 Illustration of Low Pressure Natural Convection Boiling Characteristics

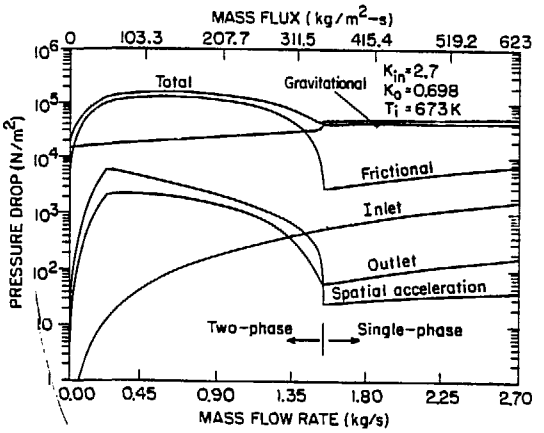

Figure 3 Pressure Drop Characteristics of Low Pressure Sodium System

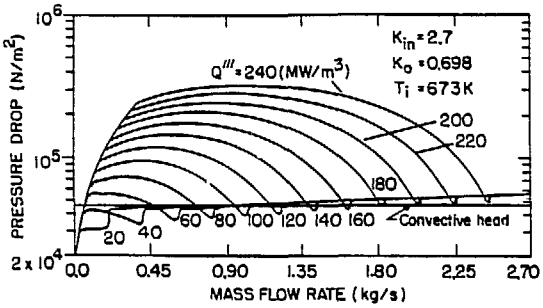

Figure 4 CRBRP Fuel Assembly Steady State Pressure Drop Vs. Flow Characteristics at Various Power Densities

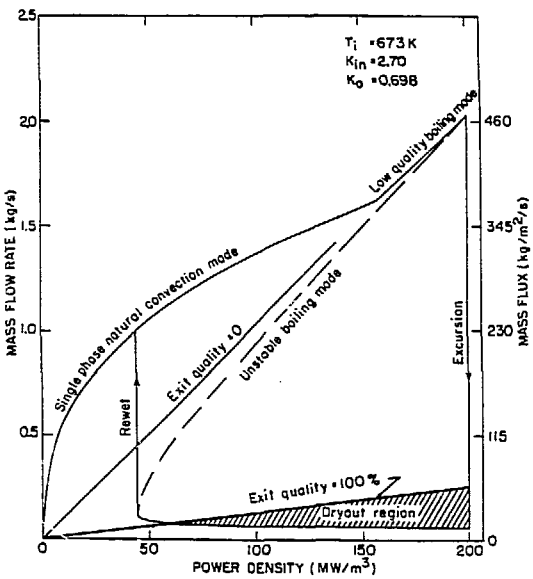

Figure 5 Boiling Map for CRBRP Fuel Assembly at 673°K Inlet Temperature

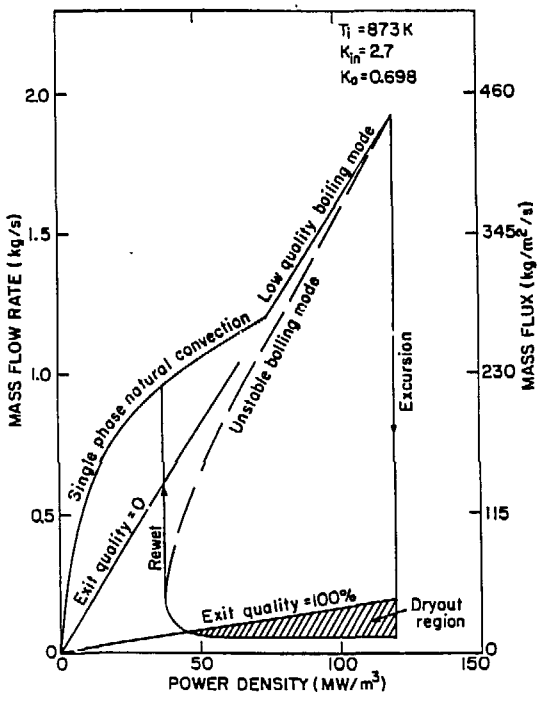

Figure 6 Boiling Map for CRBRP Fuel Assembly at 873°K Inlet Temperature

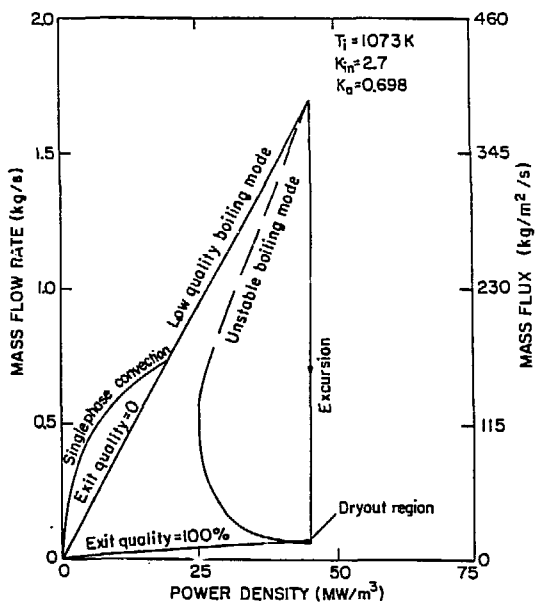

Figure 7 Boiling Map for CRBRP Fuel Assembly at 1073°K Inlet Temperature

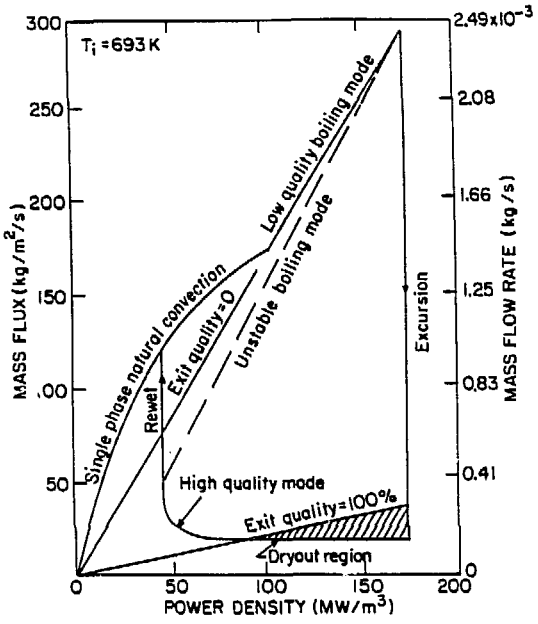

Figure 8 Boiling Map for ORNL Sodium Boiling Test Facility

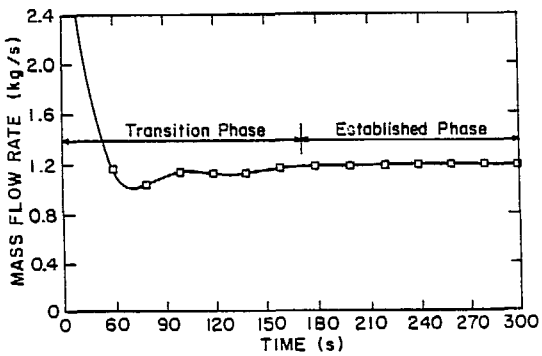

Figure 9 CRBRP Fuel Assembly Sodium Mass Flow Rate Following Loss-of-Electric Power

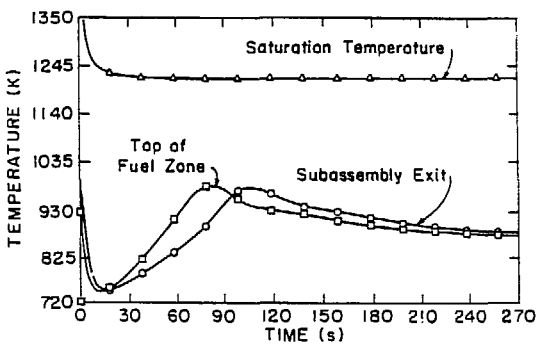

Figure 10 Fuel Assembly (Hot Channel) Sodium Temperatures (Single Phase)

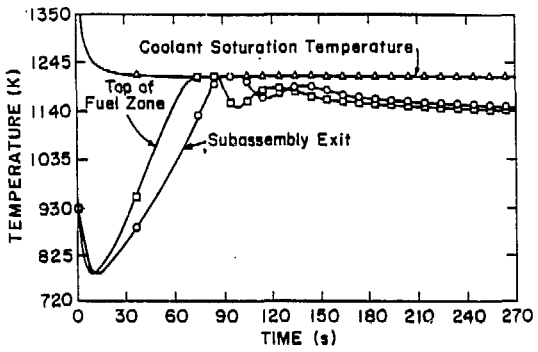

Figure 11 Fuel Assembly (Hot Channel) Sodium Temperature (With Low Quality Boiling)

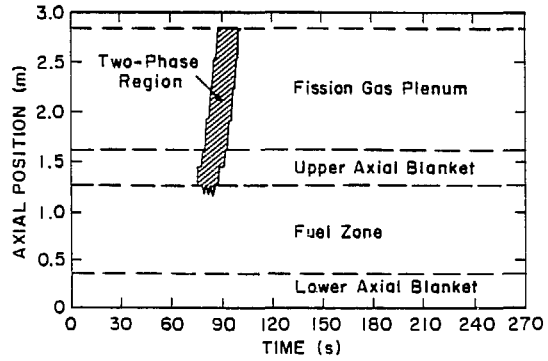

Figure 12 Axial Position of the Two-Phase Region

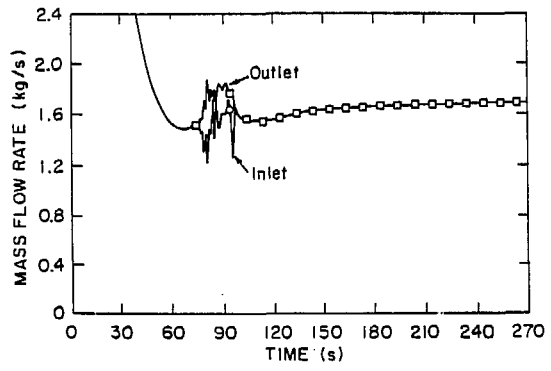

Figure 13 Fuel Assembly Inlet and Outlet Mass Flow Rates (Low Quality Boiling)

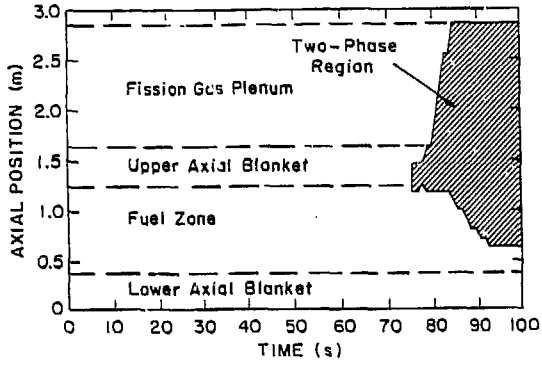

Figure 14 Axial Position of the Two-Phase Region (Unstable Boiling Leading to Excursion)

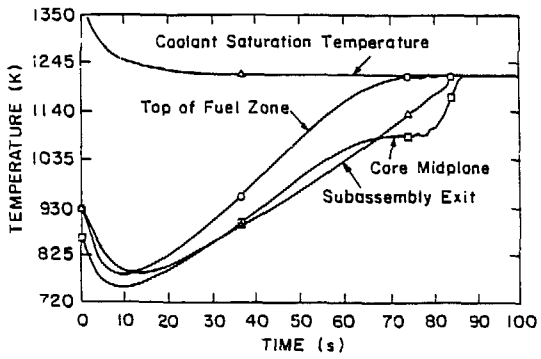

Figure 15 Fuel Assembly (Hot Channel) Sodium Temperatures (Unstable Boiling Leading to Excursion)

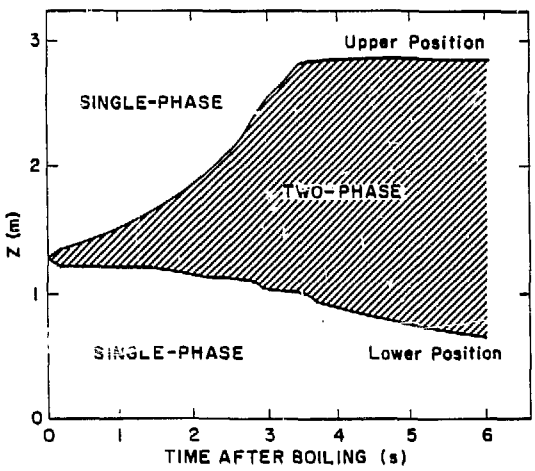

Figure 16 Axial Position of the Two-Phase Region Following Boiling Inception

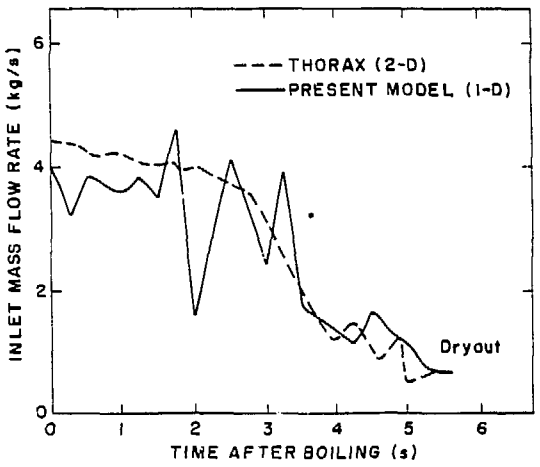

Figure 17 Assembly Inlet Mass Flow Rate Following Boiling Inception